



LUND UNIVERSITY

Snow cover and snow albedo changes in the central Andes of Chile and Argentina from daily MODIS observations (2000–2016)

Malmros, Jeppe K.; Mernild, Sebastian H.; Wilson, Ryan; Tagesson, Torbern; Fensholt, Rasmus

Published in:
Remote Sensing of Environment

DOI:
[10.1016/j.rse.2018.02.072](https://doi.org/10.1016/j.rse.2018.02.072)

2018

Document Version:
Peer reviewed version (aka post-print)

[Link to publication](#)

Citation for published version (APA):
Malmros, J. K., Mernild, S. H., Wilson, R., Tagesson, T., & Fensholt, R. (2018). Snow cover and snow albedo changes in the central Andes of Chile and Argentina from daily MODIS observations (2000–2016). *Remote Sensing of Environment*, 209, 240–252. <https://doi.org/10.1016/j.rse.2018.02.072>

Total number of authors:
5

Creative Commons License:
CC BY-NC-ND

General rights

Unless other specific re-use rights are stated the following general rights apply:
Copyright and moral rights for the publications made accessible in the public portal are retained by the authors and/or other copyright owners and it is a condition of accessing publications that users recognise and abide by the legal requirements associated with these rights.

- Users may download and print one copy of any publication from the public portal for the purpose of private study or research.
- You may not further distribute the material or use it for any profit-making activity or commercial gain
- You may freely distribute the URL identifying the publication in the public portal

Read more about Creative commons licenses: <https://creativecommons.org/licenses/>

Take down policy

If you believe that this document breaches copyright please contact us providing details, and we will remove access to the work immediately and investigate your claim.

LUND UNIVERSITY

PO Box 117
221 00 Lund
+46 46-222 00 00

1 **Snow cover and snow albedo changes in the central Andes of Chile and Argentina**
2 **from daily MODIS observations (2000–2016)**

3
4 JEPPE K. MALMROS,¹, SEBASTIAN H. MERNILD,^{2,3,4}, RYAN WILSON,⁵,
5 TORBERN TAGESSON,¹, RASMUS FENSHOLT,¹

6
7 ¹ *Department of Geosciences and Natural Resource Management, University of Copenhagen,*
8 *Copenhagen, DENMARK*

9
10 ² *Nansen Environmental and Remote Sensing Center, Bergen, NORWAY,*

11
12 ³ *Direction of Antarctic and Sub-Antarctic Programs, Universidad de Magallanes, Punta Arenas,*
13 *CHILE*

14
15 ⁴ *Faculty of Engineering and Science, Western Norway University of Applied Sciences, Sogndal,*
16 *NORWAY*

17 ⁵ *Department of Geography and Earth Sciences, Aberystwyth University, Aberystwyth, UK*

18
19
20
21
22 *Resubmitted to Remote Sensing of Environment December 12th, 2017*

23
24 **10.1016/j.j.rse.2018.02.072**

25
26
27
28
29
30
31 Corresponding author address:

- 32 Department of Geosciences and Natural Resource Management, University of Copenhagen, Øster
33 Voldgade 10, 1350 Copenhagen, Denmark.
34 E-mail: jkmalmros@gmail.com

35 **Abstract**

36 The variables of snow cover extent (SCE), snow cover duration (SCD), and snow albedo (SAL)
37 are primary factors determining the surface energy balance and hydrological response of the
38 cryosphere, influencing snow pack and glacier mass-balance, melt, and runoff conditions. This study
39 examines spatiotemporal patterns and trends in SCE, SCD, and SAL (2000–2016; 16 years) for central
40 Chilean and Argentinean Andes using the MODIS MOD10A1 C6 daily snow product. Observed
41 changes in these variables are analyzed in relation to climatic variability by using ground truth
42 observations (meteorological data from the El Yeso Embalse (EYE) weather station) and the
43 Multivariate El Niño index (MEI) data. We identified significant downward trends in both SCE and
44 SAL, especially during the onset and offset of snow seasons. SCE and SAL showed high inter-annual
45 variability which correlate significantly with MEI applied with a one-month time-lag. SCE and SCD
46 decreased by an average of $\sim 13 \pm 2 \%$ and 43 ± 20 days respectively, over the study period. Analysis of
47 spatial pattern of SCE indicates a slightly greater reduction on the eastern side ($\sim 14 \pm 2 \%$) of the
48 Andes Cordillera compared to the western side ($\sim 12 \pm 3 \%$). The downward SCE, SAL, and SCD
49 trends identified in this study are likely to have adverse impacts on downstream water resource
50 availability to agricultural and densely populated regions in central Chile and Argentina.

51
52
53
54
55
56
57
58
59
60
61
62

63 **Keywords:** Andes; Argentina; Chile; climate change; ENSO; MOD10A1; MODIS; snow albedo; snow
64 cover extent; time series analysis.

65 **1. Introduction**

66 Snow in the semi-arid mountain regions of the central Andes of Chile and Argentina provides
67 important water resources to more than 10 million people and is of major importance for agriculture in
68 this area (Masiokas et al. 2006). Moreover, snow constitutes a key seasonal component in the surface
69 energy and hydrosphere budgets, reflecting incoming solar shortwave radiation (e.g., Konzelmann and
70 Ohmura 1995). Hydrological balance in the cryosphere is highly influenced by the amount of snow
71 precipitation and the spatiotemporal variability of seasonal snow cover extent (SCE). The combined
72 variability of snow precipitation, SCE, and snow cover duration (SCD) directly influences river-runoff
73 variabilities and glacier surface-mass balance conditions (Ragetti et al. 2016; Wilson et al. 2016).

74 On high mountain glaciers, energy availability for snow and ice melt is regulated by surface
75 albedo which is defined as the ratio of incoming solar radiation reflected by a surface (Cuffey and
76 Paterson 2010). Fresh snow, for example, acts as a near perfect reflector with albedo values of up to
77 0.98. However, snow albedo (SAL) diminishes over time as a result of snow metamorphism,
78 decreasing to as low as 0.46 (Cuffey and Paterson 2010). Rainfall can further enhance this natural
79 lowering of SAL through the addition of latent energy, which can initiate melting (Benn and Evans
80 2010) and cause downwasting and thinning of glaciers (Neckel et al. 2017). Snow and ice albedo can
81 also be reduced by the surface deposition of dust and/or anthropogenic soot (Hansen and Nazarenko
82 2004; Cereceda-Balic et al. 2012). In the central Andes, an additional factor which influences SAL is
83 the seasonal formation of penitents. Often forming in areas of low humidity and high solar elevation,
84 snow penitents can result in significant changes in the surface roughness of snow-covered terrain,
85 which, in turn, influences SAL and sublimation conditions (Corripio and Purves 2006).

86 The overall variability of SAL is influenced by a variety of factors: snow grain size, levels of
87 contamination, solar zenith angle, cloud cover, snow metamorphism, surface roughness, age factor, and
88 liquid water content, amongst others (Warren and Wiscombe 1980; Mernild et al. 2015a). Since SAL is
89 a key parameter determining the amount of energy available for surface melting snow and ice, snow-
90 sublimation, and metamorphosis, spatiotemporal variability in SAL is important when determining
91 snow ablation conditions (Male and Granger 1981; Brock et al. 2000; Hock 2005; Gardner and Sharp
92 2010; Mernild et al. 2016a).

93 Spatiotemporal trends in SCE and SAL interpolated from point measurements often include
94 large errors, especially in remote mountainous regions characterized by limited ground observations,

95 localized climate conditions and complex terrain. In comparison, satellite-based remote sensing and
96 satellite derived snow cover products provide opportune sources of large-scale SCE and SAL
97 measurements and have been successfully used as key inputs in climate, atmospheric and hydrological
98 models (Farr et al. 2007; Mernild et al. 2008; Vuille et al. 2008; Mernild et al. 2015a). Remote sensing
99 systems acquiring data from the visible (VIS) to shortwave infrared (SWIR) spectrum with a high
100 temporal resolution are well suited for monitoring SCE and SAL over large areas, providing good
101 spatial and temporal coverage (Wiscombe and Warren 1980; Dozier and Frew 1981; Dubayah 1992;
102 Knap et al. 1999).

103 Several remote sensing based snow cover products are currently available, most of which apply
104 either the normalized difference snow index (NDSI) (Hall et al. 1995), empirical relationship
105 assumptions or spectral un-mixing models (Klein and Stroeve 2002a). Optical sensor systems,
106 however, are unable to acquire useful information during cloudy conditions (Justice et al. 1998;
107 Marchane et al. 2015). Therefore, frequent satellite observation revisits are essential to study changes
108 in SCE and SAL, since surface conditions can vary rapidly and may change considerably over a few
109 days.

110 To compensate for extensive cloud cover, compromises are often made by conducting satellite
111 analysis based on composite products such as the MODIS (Moderate Resolution Imaging
112 Spectroradiometer) 8 day snow cover MOD10A2 product (Hall et al. 2002), which can mask subtle
113 changes in SCE and SAL over time. In order to avoid this limitation, the MODIS MOD10A1
114 Collection 6 (C6) dataset was used this study. MOD10A1 provides daily SCE and SAL values globally
115 at a spatial resolution of 500 m, making it suitable for evaluating seasonal trends in SCE and SAL (Hall
116 et al. 2002; Liang et al. 2005; Marchane et al. 2015; Hall and Riggs 2016; Saavedra et al. 2016; Li et al.
117 2017; Huang et al. 2017; Dariane et al. 2017), snow cover phenology (Xu et al. 2017) and the relation
118 between SCE and climate (Gurung et al. 2017; Li et al. 2017). Using MOD10A1 data, this study
119 analyses spatiotemporal changes in SCE and SAL in the central Andes of Chile and Argentina by
120 parameterizing a time series of seasonal SCE and SAL metrics at the per-pixel level. Furthermore, this
121 study examines the large-scale influence of ENSO events on SCE and SAL as well as the more
122 localized effect of climatic variability (utilizing meteorological data from the El Yeso Embalse (EYE)
123 weather station) and elevation.

124

125 **2. Study area**

126 The Andes of central Chile and Argentina (31°S and 40°S) contain some of the highest peaks of
127 the entire Andes Cordillera, reaching altitudes above 6,000 m above sea level (a.s.l.) (Fig. 1). Covering
128 an area of ~1,730 km², the study area chosen is located immediately west of Santiago de Chile
129 (32°50'– 34°50'S; 69°20' – 70°40'W). This study area includes several river basins which supply
130 freshwater to large downstream populations (10+ million people in Chile and 2+ million in Argentina),
131 hydro-power stations, and agricultural lands on both sides of the cordillera (Corripio and Purves 2006).
132 This area of the central Andes also includes the largest glaciated areas in South America outside
133 southern Patagonia (Saavedra et al. 2016). River runoff in this central region originates primarily from
134 snowmelt (Masiokas et al. 2006), with snowfall contributing up to ~85 % of runoff from specific
135 catchments (Mernild et al. 2016b). The availability of snow as a freshwater resource is therefore of
136 vital socio-economic importance in this semi dry region (Peña and Nazarala 1987; Meza et al. 2012;
137 Carey et al. 2017).

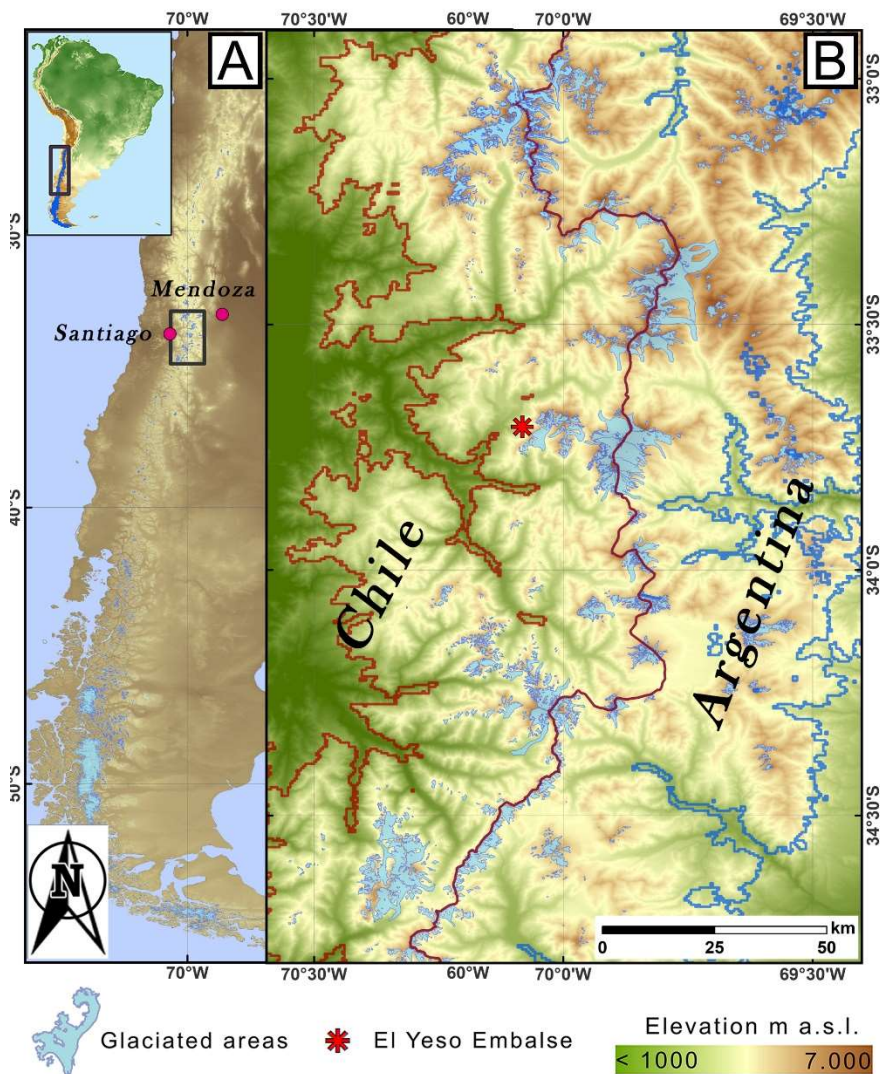
138 The intra-annual variability of precipitation in central Andes is highly influenced by the
139 placement of an atmospheric high-pressure cell over the southeastern Pacific Ocean. This cell normally
140 inhibits precipitation in the Austral summer (December – February) and allows for the passage of
141 westerlies and frontal precipitation during Austral winters (June – August) (Garreaud et al. 2009).
142 Precipitation events are usually concentrated between April and October, providing ~95 % of the mean
143 annual totals, peaking in June or July (Masiokas et al. 2016). The strength of El Niño Southern
144 Oscillation (ENSO) influences inter-annual variability in precipitation, with higher/lower precipitation
145 occurring during El Niño/La Niña events (Rutllant and Fuenzalida 1991; Escobar et al. 1995; Leiva
146 1999; Montecinos and Aceituno 2003; Garreaud et al. 2009). During El Niño events, precipitation
147 increases predominantly during the austral winter (Masiokas et al. 2006; McClung 2013). Whilst El
148 Niño events do influence precipitation amounts, these events shows little or no significant signal in
149 annual mass balance measurements of glaciers located in the central Andes but has been linked to the
150 Pacific Decadal Oscillation (PDO) rather than the ENSO (Mernild et al. 2015a).

151 Along the central Andes, annual accumulation of snow is highest at 4,000 – 5,000 m a.s.l.,
152 where glacier accumulation zones are also present (Cornwell et al. 2016; Mernild et al. 2016b; Mernild
153 et al. 2016c). Precipitation differences observed between the western and eastern sides of the Andes
154 Cordillera occur due to the combination of orographic effects of the mountain relief and the dominating

155 westerly wind direction which results in precipitation amounts and humidity being lower on the eastern
156 Cordillera slopes (Cornwell et al. 2016; Mernild et al. 2016b).

157 For the central Andes, mean surface air temperatures are normally highest between December
158 and March and lowest in July and August (Masiokas et al. 2016) and temperatures in the Andes showed
159 increasing trends from 1975 to 2006 ($\sim 0.25^{\circ}\text{C}/\text{decade}$) (Falvey and Garreaud 2009). The 0°C isotherm
160 for the western side of the cordillera (40 km northeast of Santiago de Chile), was located at 3,385 m
161 a.s.l. between 2009 and 2014 (Mernild et al. 2016c).

162



163

164 Figure 1: (a) The central Andes of Chile and Argentina; and (b) including the area of interest west and
165 east snow cover regions delineated by red and blue lines, respectively. The divide between the western

166 and eastern Andes also represents the natural border (continental divide) between Chile and Argentina.
167 Blue areas represents glaciers. The red star in the center of the study area represents the location of the
168 El Yeso Embalse (EYE) weather station.

169

170 **3. Data**

171

172 *3.1 MODIS data*

173 The MOD10A1 C6 (henceforth MOD10A1 unless other version is implied) snow product is
174 derived from daily data acquisitions by the MODIS sensor aboard the Terra spacecraft (Riggs et al.
175 2017). The MODIS global daily snow cover product MOD10A1 (MODIS/Terra Snow Cover Daily L3
176 Global 500m Grid) is derived from cloud free observations and is well suited for regional snow cover
177 and albedo mapping (Hall et al. 2002; Liang et al. 2005; Dozier et al. 2008; Rittger et al. 2013; Fausto
178 et al. 2015; Mernild et al. 2015b). The latest MOD10A1 product was released in the spring of 2016 and
179 includes a range of improvements to the previous version including, amongst others, the removal of
180 Terra sensor degradation issues and improvements in atmospheric calibration (Lyapustin et al. 2014).
181 Importantly, the algorithms used to compile the MOD10A1 snow product are modified to include only
182 the best quality observations from the atmospherically corrected MOD10GA product (Hall et al. 2002).
183 Individual MOD10A1 product parts include NDSI, NDSI snow cover (SCE), SAL and corresponding
184 quality control flags. The MOD10A1 NDSI SCE calculated is produced from an empirical relationship
185 with NDSI values, where NDSI values are multiplied by a constant (Dozier et al. 2008; Hall and Riggs
186 2016). By using only full snow cover pixels, the accuracy of the MOD10A1 SAL product is improved
187 in terms of ground truth comparisons (Sorman et al. 2007; Mernild et al. 2015b). The overall error of
188 the MOD10A1 SAL product can vary substantially but is found to be in the order of 1–10 % for good
189 observations with low atmospheric disturbances across the Greenland ice sheet (Klein and Stroeve
190 2002b). The overall error at this location is likely to be higher due to the complex terrain of the Andes
191 Mountains. However, changes in albedo can still be quantified and here we opted for a per-pixel
192 temporal change analysis that is expected to mitigate the influence of topography to some degree by
193 avoiding direct inter-comparison of pixels influenced by different slope/aspect.

194 MOD10A1 data used in this study was obtained from the NASA Earth Observation System
195 Data and Information System (EOSDIS) Reverb ECHO website (<https://reverb.echo.nasa.gov/>). Out of

196 the 5,844 potential scenes available between March 1 2000 and Feb 29 2016, only 121 (~2 %) were
197 missing in the archive, with a maximum temporal gap of 17 days. The snow cover year (season) was
198 set to start 1 March and end February 28 (29) based on analysis of the data set. Pixels with cloud cover
199 or poor retrievals were omitted as determined from QA flags and only pixels flagged as “best quality”
200 were included in the further analysis (see section 4.1). Out of all pixels in the data series 74.8 %
201 contained “best quality” data (supplementary material S1).

202

203

204 *3.2 Ancillary data*

205 Elevation data were obtained from the Shuttle Radar Topography Mission (SRTM) v.3. SRTM
206 provides elevation data at a spatial resolution of 30 meters with an overall vertical accuracy of ~10 m
207 and geo-position error of ~9 m (Farr et al. 2007). Multivariate El Niño index (MEI) ranks were
208 obtained from the National Oceanic and Atmospheric Administration (NOAA) website
209 (<http://www.esrl.noaa.gov/psd/enso/mei/table.html>). The MEI provides a ranked index of the strength
210 of El Niño and La Nina events. MEI values are normalized for each bimonthly season (Wolter and
211 Timlin 2011) and cover the 16-year study period of snow cover and snow albedo observations.

212 We acquired mean monthly air temperature (MMAT), mean annual air temperature (MAAT),
213 and monthly precipitation sums (2000–2016) from the El Yeso Embalse meteorological station (EYE)
214 (location in Fig. 1; data shown in supplementary material S2) from Dirección General de Aguas (DGA;
215 www.dga.cl). Finally, glacier outlines were obtained from the Randolph glacier inventory v. 5.0
216 (Pfeffer et al. 2014) in combination with updated glacier shapes from 2013/2014 (Malmros et al. 2016).

217

218 **4. Methods**

219

220 *4.1 Time series preprocessing*

221 The MOD10A1 time series was preprocessed and analyzed using the program TIMESAT
222 (Jönsson and Eklundh 2002, 2004; Eklundh and Jönsson 2015). TIMESAT originally developed to
223 analyze vegetation seasonality can be applied to all remote sensing data containing seasonal variability.
224 We applied a Savitzky-Golay filter within TIMESAT which allows for a smoothing of the
225 MOD10A1 time-series by applying polynomial fitting to the data points within a moving window of a

226 certain width (Savitzky and Golay 1964; Jönsson and Eklundh 2004). Missing dates were filled with
 227 blank scenes before smoothing (Jönsson and Eklundh 2002) in order to compose a complete time
 228 series. Pixels not flagged as “best quality”, as determined from QA flags, were given a weight of zero
 229 in the fitting algorithm to allow only pixels of best quality to be included. The width of the moving
 230 window influences the degree of smoothing and the ability of the filter to cope with rapid changes
 231 (parameters used in the TIMESAT preprocessing are shown in Table 1). The polynomial fitting was
 232 iterated and adapted to the upper part of the curve by assigning weights to data points above and below
 233 the result of the previous step (Jönsson and Eklundh 2004). SCD was extracted in TIMESAT for SCE,
 234 and the seasonal snow cover integral (SCI) (defined as the integral under the curve between onset and
 235 end of seasonal snow cover) was extracted to evaluate the accumulated seasonal SCE for each season.
 236 Areas characterized by limited seasonal variability were masked out due to the inability of the
 237 TIMESAT algorithm to estimate SCD for such conditions. The mask was created from the median of
 238 the 16 seasons and excluded areas with less than 16 days in the SCD dataset. Most excluded areas were
 239 located in glacier accumulation zones where constant snow cover prevents seasonal variability in SCE.

240

241 Table 1: Input parameters for use in TIMESAT.

Parameter	NDSI Snow Cover	Snow Albedo
Seasonal parameter	0.7	0.7
Number of envelope iterations	3	3
Adaptation strength	2	2
Savitzky-Golay window size	15	15
Spike Method	Median filter	Median filter
Amplitude season start (%)	70	65
Amplitude season end (%)	20	46

242

243 *4.2 Trend estimation*

244 We conducted linear temporal trend analysis to estimate the magnitude and direction of changes
 245 in SCE, SAL, SCD, SCI, MAAT, and annual precipitation. We calculated per-pixel trends by applying
 246 a nonparametric linear regression model with time as the independent variable and the abovementioned
 247 variables as dependent variables. Since time series of the variables analyzed often do not meet

248 parametric assumptions of normality and homoscedasticity, a median trend (Theil–Sen, TS) procedure
249 was applied using the Theil-Sen slope estimator (median trend) which has proven robust against
250 outliers (Eastman 2009). Uncertainty estimates of trends are calculated from standard deviations of the
251 calculated metrics and are provided as \pm values to all trends reported. The significance of the trends
252 was determined using the nonparametric Mann–Kendall test of significance (Mann 1945; Kendall
253 1975). The Mann–Kendall significance test is commonly used as a trend test for the TS median slope
254 operator (Eastman 2009) and produces outputs of z-scores that allow for the assessment of both the
255 significance and direction of trends. The trends were considered significant at $p < 0.05$ (where p
256 denotes the probability that there is no significant difference between observations over time). Trends
257 in SCE, SCD, and SCI were extracted from the area of maximum values (minimum of 75% at any
258 given time) for the entire study period and similar for SAL.

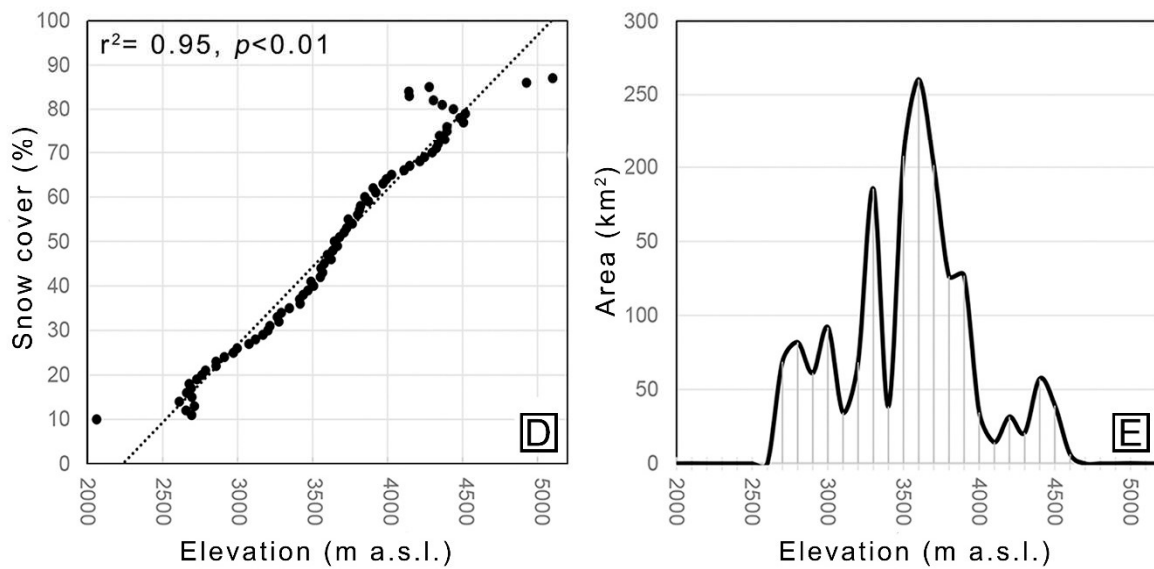
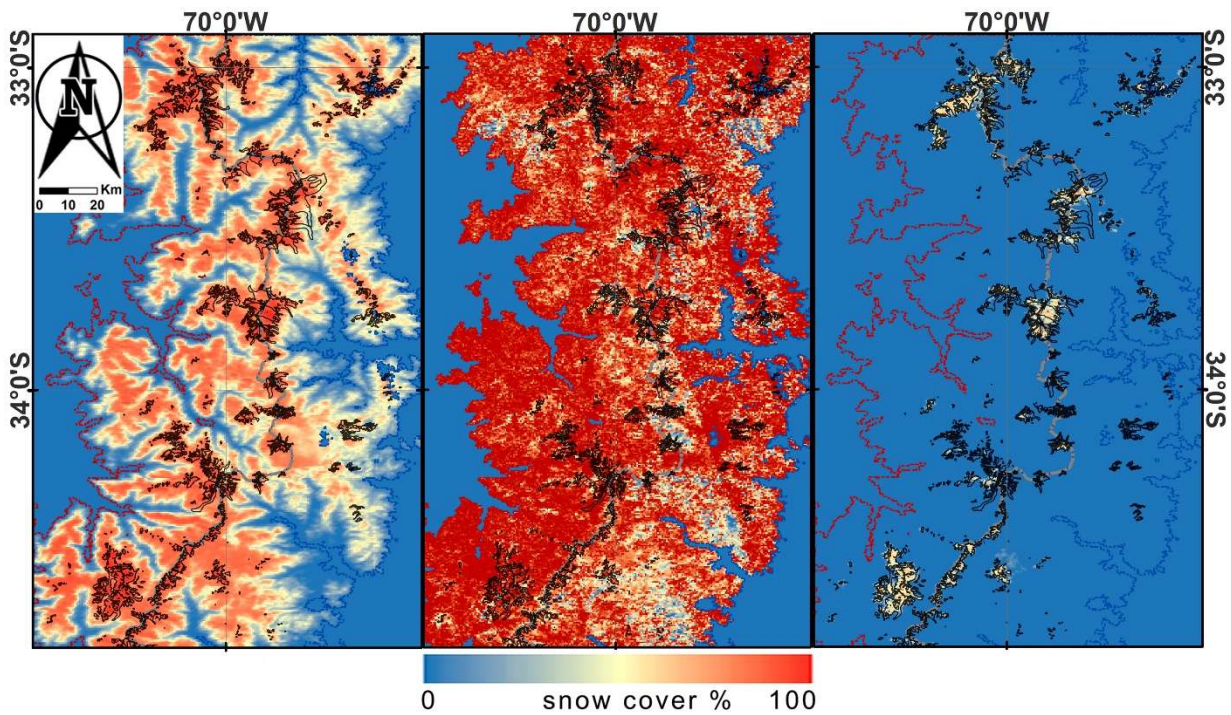
259

260 **5. Results**

261 *5.1 Spatio-temporal patterns in snow cover extent*

262 Statistical analysis of the MODIS time series revealed that the minimum, median, and
263 maximum SCE for the entire observation period and area (Fig. 2) was 2 %, 43 %, and 74 %,
264 respectively. SCE showed the presence of a clear linear relationship with elevation (coefficient of
265 determination (r^2) = 0.95, $p < 0.01$; Fig. 2d). However, the relationship was imperfect ($r^2 = 0.34$) above
266 4,000 m a.s.l due to increased scattering in the accumulation zone of the glaciers. At its maximum, SCE
267 covered 1,730 km² (74%) of the study area, only being present at elevations above 1,250 m a.s.l. SCE
268 area was normally distributed with highest concentration of SCE observed between 3,250 and 4,000 m
269 a.s.l. (Fig. 2e). SCE was on average ~11 % less on the eastern side of the Cordillera compared to the
270 west (Fig. 2a-c).

271



272

273 Figure 2: a) Median snow extent; b) maximum snow cover extent; c) minimum snow cover extent for
 274 the 16 snow seasons observed (2000–2016) (glaciers are delineated by black); d) Mean SCE change
 275 with elevation; and e) Snow covered area distribution with elevation.

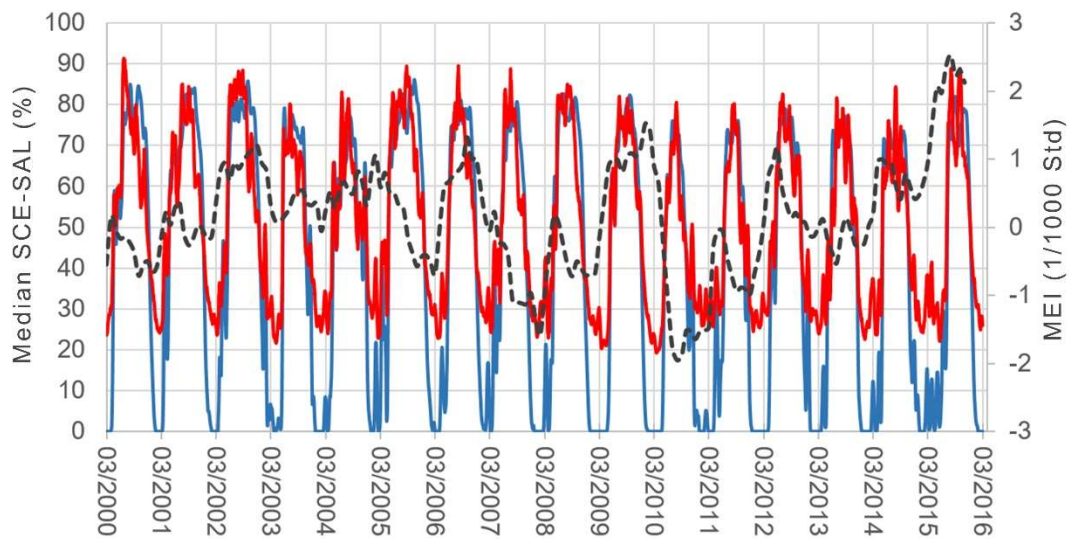
276

277 *5.2 Inter- and intra-annual variability in snow cover extent (SCE) and snow albedo (SAL)*

278

279 The mean SCE over the study area between 2000 and 2016 was approximately ~25 % in austral
 280 summer and ~68 % in austral winter, reaching a maximum between July 24th and 25th October and a
 281 minimum in autumn between March 6th and June 6th (Fig. 3). Overall, spatial trends for SCE and SAL
 282 showed widespread downward tendencies (Fig. 4). For SCE, downward trends dominated, with
 283 medium SCE decreasing by 13.4 ± 4.0 % between 2000 and 2016 (0.35 % yr^{-1}). Demonstrating spatial
 284 variabilities, the downward trends in SCE were found to be more pronounced for the the eastern side of
 285 the Cordillera (13.9 ± 4.0 %, 0.9 % yr^{-1}) compared to the west (12.4 ± 3.1 %, 0.8 % yr^{-1}). The eastern side
 286 of the Cordillera also showed lower SCE but higher SCE variability compared to the western side, this
 287 despite the eastern side being more elevated (mean elevation for the western and eastern sides is 3,115
 288 m a.s.l and 3,720 m a.s.l, respectively) (Fig. 2d). Median SAL trends from March 2000 to February
 289 2016 were also downward with mean values decreasing by 7.4 ± 2.2 % (0.5 % yr^{-1}). Downward trends in
 290 SAL were shown to be more widespread in the southern parts of the study area compared to northern
 291 parts. However, we found no significant differences between the eastern and western sides of the
 292 Cordillera.

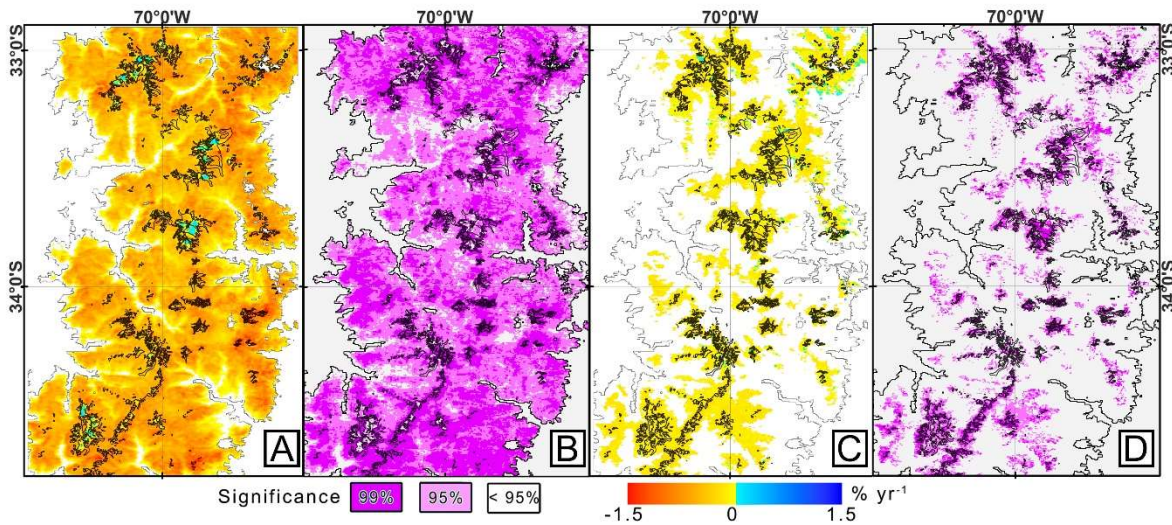
293



294

295 Figure 3: Variation in daily median SCE (blue) and median SAL (red) percentage and the bi-monthly
 296 multivariate ENSO index (MEI) (dark dashed line) in 1/1000 standard variations (Wolter and Timlin
 297 2011).

298



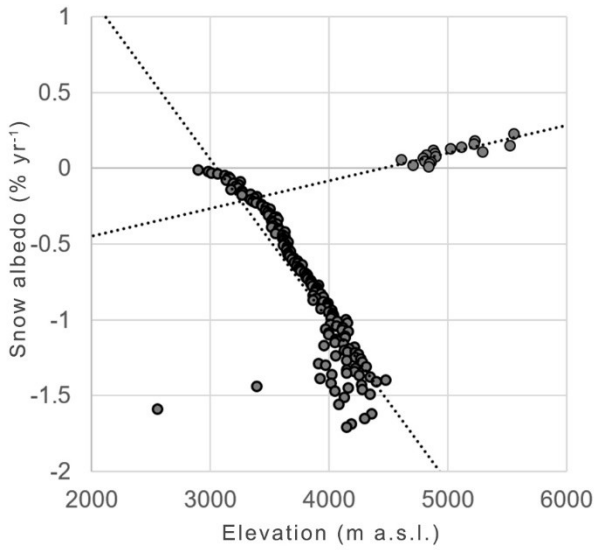
299

300 Figure 4: Linear median trend ($p < 0.05$) in: SCE (a) and SAL (c) from Mar 2000 through Feb 2016, and
 301 the corresponding significance level of each trend (b, d).

302

303 Comparisons with SRTM data, the SAL trends observed showed negative correlations below $\sim 4,600$ m
 304 a.s.l. (-1.1 ± 0.8 % yr⁻¹, $r = 0.84$, $p < 0.01$). Above $\sim 4,600$ m a.s.l., however, a distinct shift is observed,
 305 with increasing correlations as a function of elevation (0.2 ± 0.01 % yr⁻¹, $r = 0.83$, $p < 0.01$) (Fig. 5). In
 306 regards to intra-annual variability, SCE showed pronounced downward trends (< -1 % yr⁻¹) during the
 307 onset (April, May, and June) and offset (October, November, December, and January) of the snowy
 308 season. In comparison to SCE, SAL showed slightly less intra-annual variability with most downward
 309 trends occurring during the onset of the snowy season (Fig. 6).

310

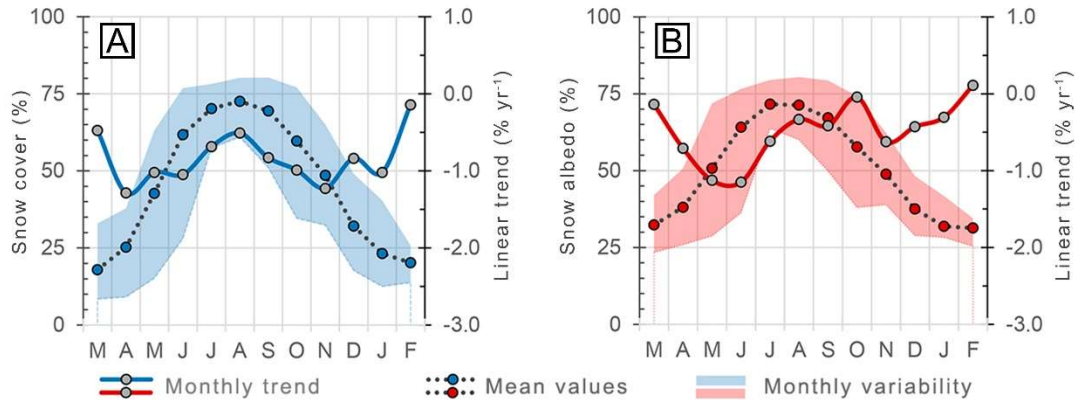


311

312 Figure 5: Trends in snow albedo (SAL) with elevation.

313

314



315

316 Figure 6: Intra-annual linear trends (blue and red lines), monthly mean values (dotted lines) and spread
 317 (colored areas; monthly minimum and maximum values)) in: (a) snow cover extent (SCE); and (b)
 318 snow albedo (SAL) between 2000 and 2016.

319

320 5.3 Snow cover duration (SCD) and seasonal snow cover integral (SCI)

321

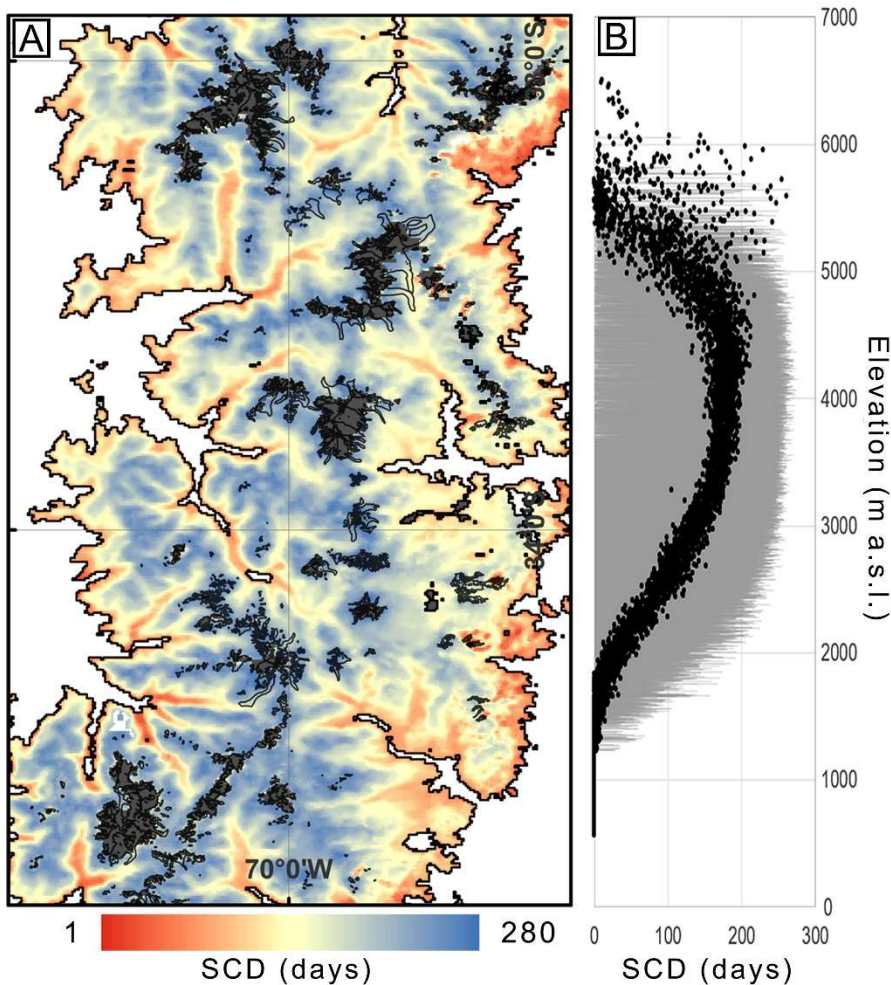
322

323

324

The seasonal SCD values ranged between 0 and 280 days and the seasonal mean SCD ranged between 203 days in the 2005–2006 to 130 days in 2011–2012, with an overall median of 173 days (Fig. 7a). We observed a strong correlation between SCD and elevation (excluding glacier areas). SCD, for example was shown to increase by an average of ~6 days for every 100-meter increment within the

325 2,000 to 4,600 m a.s.l. elevation range ($r^2=0.80$, $p<0.01$) (Fig. 7a). Overall, the trends in SCD were
 326 downward, showing a mean reduction of 43 ± 20 days for the study period (-2.7 ± 1.3 days yr^{-1}) (Fig.
 327 8a). Trends were especially negative on the eastern side of the Cordillera, with a reduction of 52 ± 36
 328 days (3.3 ± 2.3 days yr^{-1}), whereas on the western side SCD reduced by 35 ± 33 days (2.2 ± 2.0 days yr^{-1}).
 329
 330



331
 332 Figure 7: a) Median snow cover duration (SCD, days) 2000–2016 (dark grey areas represent locations
 333 where the model failed to determine seasonality); and (b) Mean snow cover duration with elevation for
 334 the 2000–2016 period (grey bars show the spread between minimum and maximum values of SCD as a
 335 function of elevation).
 336

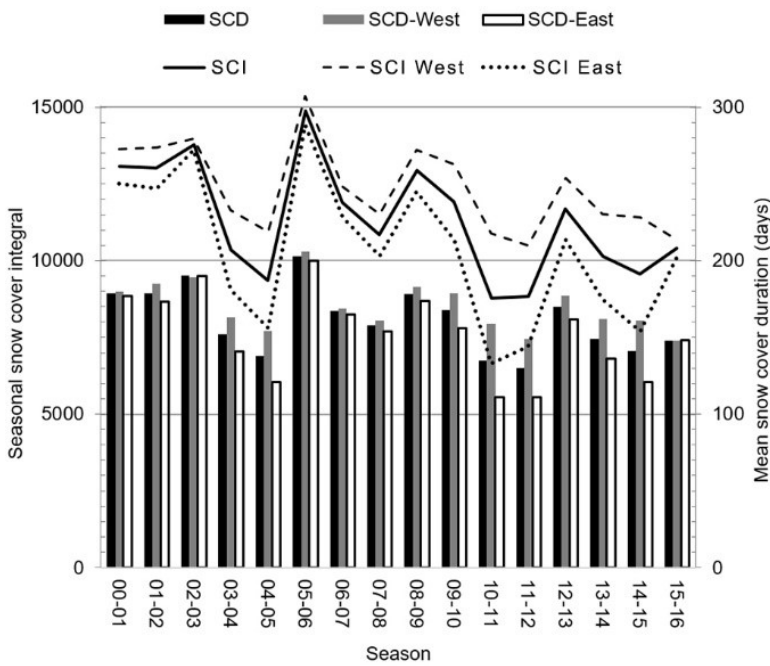
337

338 Figure 8: (a) Per pixel yearly snow cover duration (SCD) trend 2000–2016, and (b) corresponding
339 significance of trend. Dark gray masked areas represent the mask where SCD values are erroneous and
340 black lines represent glaciers.

341

342 The SCI for the entire study area declined by $1.5 \pm 0.5 \text{ \% yr}^{-1}$ (median trend), corresponding to 25 ± 8
343 % during the full period of 16 snow seasons. The SCI also shows substantial inter-annual variation
344 (Fig. 9), especially on the eastern side of the Cordillera, where SCI is on average 17 % smaller and
345 trends are substantially more downward ($1.8 \pm 0.5 \text{ \% yr}^{-1}$) than for the western side ($1.2 \pm 0.4 \text{ \% yr}^{-1}$).

346



347

348 Figure 9: Mean snow cover duration (SCD, bars) and seasonal snow cover integral (SCI, lines) for the
349 entire study area and for the western (SCD-W) and eastern (SCD-E) sides of the cordillera separately.

350

351 5.4 Impact of changes in temperature, precipitation, and El Niño Southern Oscillation (ENSO) on snow 352 cover duration and snow albedo

353

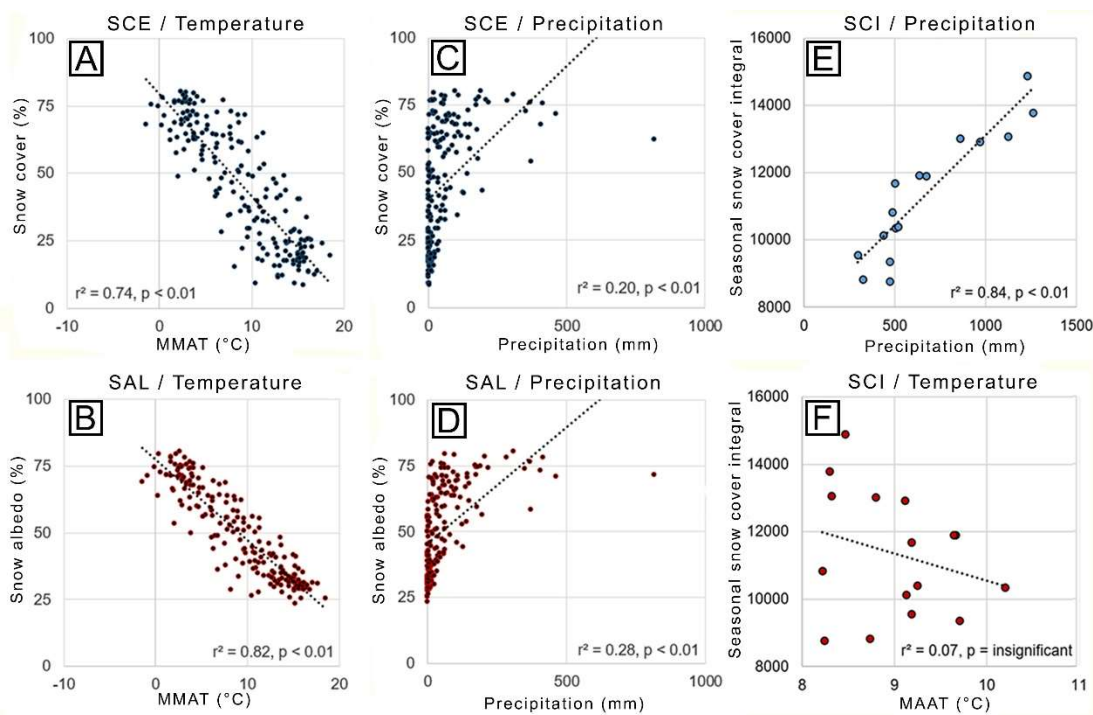
354 Analysis of the meteorological data available from the EYE weather station (Figure 1b)

revealed a significant downward trend in precipitation of -4 mm yr^{-1} and an insignificant trend in

355 MAAT of $0.05^{\circ}\text{C yr}^{-1}$ between 2000 and 2016. Between 2000 and 2009, nine extreme precipitation
 356 events ($>200\text{ mm month}^{-1}$) were identified, with the 2003-2004 season (March-February) receiving a
 357 maximum of 1,259 mm. These ‘extreme’ events occurred mostly during austral winters and account for
 358 large differences in inter-annual precipitation amounts, SCE and SCD sums. Post 2009, no extreme
 359 precipitation events occurred, however a minimum of 317 mm was observed for the 2014-2015 season.
 360 The mean annual precipitation sum for the 2000 to 2016 observation period was 677 mm. MAAT for
 361 this observation period was 9.0°C , with maximum and minimum values of 10.3°C and 7.3°C measured
 362 for the 2003-2004 and 2011-2012 seasons, respectively.

363 Statistical comparisons between the MODIS-derived snow data and the observed EYE
 364 meteorological data revealed that monthly SCE and SAL averaged over the study area correlated
 365 strongly with MMAT (r^2 -values of 0.74 and 0.84, respectively) (Fig. 10a-b). Mean monthly SCE and
 366 SAL also correlate with monthly precipitation sums, but to a lesser extent (r^2 -values of 0.20 and 0.28)
 367 (Fig. 10c-d). In comparison, SCI correlated more strongly with annual precipitation sums (r^2 -value of
 368 0.84) (Fig. 10e).

369



370

371 Figure 10: Relationships between monthly meteorological data (EYE station; Fig. 1) and monthly SCE,
 372 monthly SAL, and SCI averaged over the study area. a) Monthly SCE against MMAT; b) monthly SAL

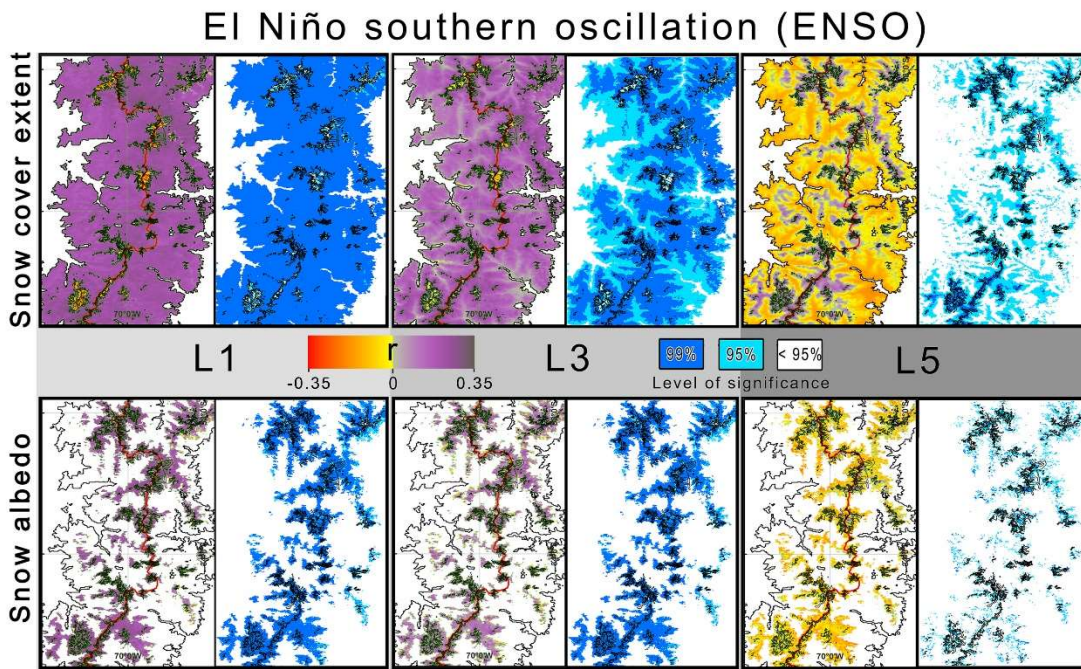
373 against MMAT, c) Monthly SCE against monthly precipitation sums, d) Monthly SCE against monthly
 374 precipitation sums, e) SCI against annual precipitation sums, and f) SCI against MAAT.

375

376 ENSO events (MEI) (plotted in Fig. 3) show significant correlations with mean SCE and SAL
 377 values for the study area (Fig. 11). Mean correlation coefficient values (r) between MEI and SCE/SAL
 378 were strongest when a lag of one month (L1) was applied to the SCE/SAL time series (mean r -values
 379 of 0.21 for the study area).

380 Generally, glaciated areas where snow cover is already present are characterized by negative
 381 SCE and ENSO correlations for shorter lag periods (L1), which is in contrast to the surrounding snow
 382 covered areas. This pattern is reversed for longer lag periods (e.g., five months), when glaciated and
 383 higher elevated areas significantly correlate with ENSO, whereas surrounding lower altitude areas are
 384 characterized by negative correlations.

385



386

387 Figure 11: Per-pixel correlations and significance of SCE/SAL with the ENSO index (MEI) including
 388 one-, three- and five-month lag time (L1, L3, and L5). Red line demarks the east west divide.

389

390 **6. Discussion**

391

392 *6.1 Monitoring and assessment of snow cover and snow albedo*

393 Spatio-temporal analysis of MODIS-derived SCE, SAL, SCD, and SCI data revealed significant
394 changes during the observation period of this study. Key to the interpretation of these results is the
395 quantification of sensor related errors and their influence on the trends observed (2000–2016).
396 Unfortunately, only a few validation studies of the MOD10A1 C6 products have been published to
397 date. Recent studies using MOD10A1 collection C6 for the Greenland ice sheet however found that
398 v.C6 corrects for the C5 temporal trend bias in dry snow areas and that albedo retrieval accuracy in C6
399 is substantially improved over C5 (Box et al. 2017; Casey et al. 2017). Therefore, the accuracy of this
400 product is expected to be better than or at least as good as the C5 product, which has been evaluated in
401 several previous studies (Tekeli et al. 2005; Hall and Riggs 2007; Gao et al. 2010; Arsenault et al.
402 2014; Marchane et al. 2015). These studies estimate an overall detection error ranging from ~5 % to
403 ~48 %, depending on locational properties and type of ‘ground truth’ observations used. In general,
404 spatially homogeneous locations with flat terrain produces less error than in complex terrain with
405 mixed surface as being the case for this study (Wang et al. 2014; Burakowski et al. 2015; Moustafa et
406 al. 2017). By applying a per-pixel temporal change analysis approach in the current study, thereby
407 avoiding direct inter-comparison of pixels characterized by different slope/aspect, the influence of
408 topography is expected to be reduced to some degree. This should also be seen in the context of the
409 latitudinal location of the study area (32°50’– 34°50’ S), characterized by an annual range in solar
410 zenith angles of 28-60 for MODIS overpass times. This makes the region less prone to influences from
411 mountain shadowing as compared to complex terrain of higher latitudes of the northern/southern
412 hemisphere. Snow detection in v.6 is expected to show improvements in comparison to previous
413 versions especially above 1.300 m a.s.l., where the surface temperature screen used in the product
414 algorithm (which has previously caused false negatives) has been rolled back leaving fewer gaps in the
415 data (Hall and Riggs 2016).

416 The smoothed and gap-filled MOD10A1 C6 dataset produced with TIMESAT is assumed to
417 correctly represent the seasonal snow distribution for the area. Here, only the best quality MOD10A1
418 C6 observations (by including information available from the QA flags; 0=“best quality”) were used
419 for the Savitzky-Golay function fitting in TIMESAT. By adjusting the data fitting to the upper
420 envelope of the daily observations, we ensured that the SCE and SAL values follow rapid changes,

421 which can occur in snow cover extent and albedo. The TIMESAT model uses local function fitting,
422 where values before and after in the time series are considered. This local function fitting reduces the
423 chance of error occurrence in the MOD10A1 observed snow cover (Tekeli et al. 2005). For the upper
424 ablation zones of glaciers, characterized by limited seasonal variability or year round snow SCE, it is
425 not possible to accurately assess seasonality variables and thereby SCD. In this case, a glacier mask
426 was applied based on SCE seasonal variability, in doing so, restricting the SCD analysis to non-
427 glaciated areas (Fig. 7a). Out of all the pixels in the data series 24.2 % was filled with modeled data
428 from TIMESAT.

429 Snow albedo detection in mountainous environments from remotely sensed imagery can contain
430 large errors when measured on terrain with steep slopes. Validation of satellite or aerial imagery based
431 data using stationary point albedometers can also be challenging because of pronounced mixed pixel
432 and geolocation issues (Liang et al. 2005; Sorman et al. 2007; Mernild et al. 2015b; Box et al. 2017).
433 However, these issues are not likely to have significantly influenced the trends observed in this study as
434 the MOD10A1 pixels are measured in the same pixel location from year to year in a location where
435 seasonal variation in solar zenith angle influence is relatively low (annual range between 28-60
436 degrees) compared to higher latitudes of the northern/southern hemisphere. MOD10A1 snow albedo is
437 produced only for cloud free pixels with full snow cover (+50 %) indicating that for pixels
438 characterized by limited full snow cover observations seasonal fitting could have influenced the
439 accuracy of the TIMESAT generated data.

440

441 *6.2 Analysis of climate variables*

442 The analysis of the effect of local scale climatic variability presented in this study made use of
443 the only existing weather station EYE in the study area. Indeed, the use of a single station is not ideal
444 when comparing measurements with the spatially large-scale MOD10A1 dataset. Furthermore, given
445 the location of this weather station on the western side of the cordillera and the presence of distinct
446 climatic gradients (e.g. Mernild et al. 2016a), the data recorded is unlikely to be fully representative of
447 the study area as a whole. However, this scarce coverage of ground observations reflects the general
448 conditions for mountainous areas of the Andes and underlines the need for remotely sensed monitoring
449 methods.

450 Upward trends in MAAT have higher impact the lower the altitudes (mostly noticeable in the
451 southern part of the study area) causing changes in onset and offset of snow seasons to be more
452 sensitive to even small changes in temperature (Fig. 4). Low areas with small slope gradient show
453 higher sensitivity to upward changes in MAAT in regards to snow accumulation. Especially the low
454 elevated areas on the eastern side of the cordillera show the effect of increased MAAT.

455 Above 4,600 m a.s.l., SCD shows a considerable increase in variability (Fig. 7b). This however
456 is not surprising as, in highly elevated zones where SCD can be dependent on localized terrain (slope
457 and area of topographical shadow) and weather conditions. High wind speeds, for example, often make
458 it less likely for snow cover to persist in certain areas despite high levels of solid precipitation.

459

460 *6.3 Drivers of change on snow cover variables*

461 Studies based on modeling, field measurements and remote sensing have provided insights into
462 the past, current, and future impacts of climate change on snow conditions and runoff in the Andean
463 river catchments of central Chile and Argentina (Pellicciotti et al. 2007; Apaloo et al. 2012; Delbart et
464 al. 2015; Mernild et al. 2015a, 2016a, 2016c; Ragetti et al. 2016). A number of these studies have
465 predicted that air temperatures in the central Andes will continue to increase. An increase in air
466 temperature, together with seasonal changes in precipitation patterns, will likely result in a decrease in
467 the amount of runoff from snow melt and an increase in the amount of runoff from rain (Cai et al.
468 2014; Mernild et al. 2016a, 2016c; Ragetti et al. 2016). Since the 1970's, precipitation events have
469 generally become more intense but less frequent in central Chile (Falvey and Garreaud 2007; Garreaud
470 et al. 2009). The EYE precipitation data, for example, shows a number of intense precipitation events
471 (above 200 mm m⁻¹) during the 2000–2009 period. Interestingly, none of these 'intense' events
472 occurred during the 2010–2016 period.

473 Per-pixel correlations between SCE/SAL and the Multivariate El Niño index (MEI) show that
474 MEI has a strong and significant impact on inter-annual SCE/SAL variability in the region (Fig. 11).
475 Although El Niño events are often associated with increases in precipitation, they can also be
476 associated with increases in air temperature (Cai et al. 2014) which, together, can have a pronounced
477 altitude dependent effect on snow cover during spring and autumn. An increase in air temperature, for
478 example, causes the 0°C isotherm to ascend to higher elevations resulting in a larger proportion of
479 precipitation falling as rain as opposed to snow. Mernild et al. (2016c) observed this phenomenon for

480 the Olivares basin (33°12' S; 70°09' W) between 1979 and 2014, where precipitation has been
481 increasingly falling as rain in recent years. This change in the partitioning of precipitation over
482 mountainous areas can offset the positive effects of increased precipitation on snow accumulation, with
483 rainfall often enhancing snow and ice melt rates on glacier surfaces. The significant spatial variation in
484 correlation between MEI and SCE for one-month lag, we suspect is caused by the presence of snow
485 cover on glaciers giving negative or no correlation on short term but increasing correlations with time.

486 Reduction in SCE in this study has also been studied in modelling studies based on MERRA
487 satellite data (Mernild et al. 2016b, 2016c) which estimate that snow cover extent in the central Andes
488 has reduced ~1.3% per decade 2000–2014 (linear trend, for the b1 window in Fig. 1) (Mernild et al.
489 2016b). Mernild et al. (2016c) suggest that the largest decreases in snow cover have occurred within
490 the 3,000–5,000 m a.s.l. elevation range, where more than 70 % of seasonal precipitation falls as snow.
491 In comparison, the rate of SCE change observed in this study for the same period and area is
492 significantly higher, with per decade reductions equating to ~2.8%. This difference between the results
493 presented here and in Mernild et al. (2016c) may either be an indicator of faster SCE reduction during
494 the 2000–2016 period or highlight possible SCE overestimations in the MERRA model utilized by the
495 latter. For other regions of the world snow cover reductions are well documented. In the Arctic, for
496 example, a general decrease in the amount of snow has been observed between 1999 and 2009, together
497 with reductions in maximum winter snow water equivalent, a later snow-cover onset in autumn and
498 earlier snow-free date in spring, and a decreasing snow-cover duration (Liston and Hiemstra 2011).
499 To sustain all year runoff, rivers of the central Andes rely on substantial contributions from snow and
500 ice-melt, and river discharge here is strongly linked to snow cover changes (Delbart et al. 2015).
501 Decreases in SCE at the magnitudes shown in this study has the potential to cause a substantial
502 redistribution in seasonal runoff for this region, where ~21 % of river runoff originates from snow- and
503 ice- melt (increasing to ~85 % during dry summers) (Peña and Nazarala 1987; Mernild et al. 2016a).
504 Glaciers in the central Andes are shrinking and down wasting as a consequence of climate warming and
505 changes in precipitation patterns (Masiokas et al. 2006; Bodin et al. 2010; Gacitua et al. 2015; Malmros
506 et al. 2016). Although initially increasing, ice melt runoff will begin to reduce in the future as lowest
507 elevation land ice disappears. If these ice/snow cover trends continue, runoff conditions will likely
508 change, especially during spring, dry summers and periods of drought, affecting the future
509 sustainability of freshwater resources in areas downstream of the central Andes (Peña and Nazarala

510 1987; Delbart et al. 2015; Saavedra et al. 2016; Carey et al. 2017; López-Moreno et al. 2017). Whether
511 this change in runoff will cause the low lying areas in the catchment to become wetter or drier is
512 largely determined by local topography (Polk et al. 2017, López-Moreno et al. 2017).

513 Directly influencing the surface energy balance, the downward trends in SAL revealed in this
514 study (Fig. 4) may possibly result in positive feedbacks in regards to snow and ice melt. This trend of
515 darkening surfaces, either from reduced snow cover or from enhanced melt conditions, is likely to be
516 reinforced by increasing air temperatures and decreasing precipitation (e.g., Mernild et al. 2016c).
517 Another positive feedback could be initiated by the accumulation of dust and debris on glacier surfaces
518 leading to more energy being absorbed and further melt conditions, especially on lower parts of
519 glaciers (Hansen and Nazarenko 2004; Oerlemans et al. 2009; Arenson et al. 2015). Minimum glacier-
520 wide albedo has shown to be a good predictor for glacier mass balances conditions for temperate
521 glaciers (López-Moreno et al. 2017; Polk et al. 2017), which suggests that glaciers in the study area
522 may have positive mass balances, at least for some of the years analyzed. Decreases in surface albedo
523 have also been observed for many other glaciated parts of the world (Box et al. 2012; Tedesco et al.
524 2013; Abermann et al. 2014; Fausto et al. 2015; Mernild et al. 2015b). The mean albedo for the
525 Greenland ice sheet ablation area (June–August), for example, declined by 22.9 % from 2000 to 2016
526 while dry snow areas only decreased by 1.2 % (Box et al. 2017). Increasing albedo values seen above
527 4.600 m a.s.l. (Fig. 5.) are likely contributed to by the increase in precipitation and the presence of dry
528 snow conditions at high altitudes (Box et al. 2017).

529 The central Andes are dominated by two distinctly different climate systems. On the western
530 side of the Cordillera the climate is influenced by oceanic atmospheric interactions, whereas on the
531 eastern side the climate can be considered continental in type (Prohaska 1976). This difference in
532 climate is highlighted in this study by the relatively weak correlation between SCE/SAL and MEI on
533 the eastern side of the Cordillera compared to the west. A higher inter-annual variability in SCE and
534 SCI and more downward trend on the eastern part may be contributed to continental climate conditions
535 (Fig. 9) as also observed in Saavedra et al. 2017.

536

537 **7. Conclusions and outlook**

538 Overall, snow cover extent (SCE) and snow albedo (SAL) decreased by 13.4 ± 4 % and 7.4 ± 2
539 %, respectively, between 2000 and 2016. SCE showed more downward trends on the eastern side of the

540 Andes Cordillera ($13.9 \pm 4 \%$), while SAL showed a uniform decline throughout the area. A seasonal
541 analysis revealed downward trends in SCE and SAL for all months of the year, with the largest
542 decreases occurring during the onset (for SCE and SAL) and at the end of the snow seasons (for SCE)
543 ($> 1\% \text{ yr}^{-1}$). SCE showed a near linear increase with elevation ($r^2=0.96$, $p < 0.01$), and largest relative
544 losses occurring at elevations above 4.600 m a.s.l. outside glaciated areas. Spatial analysis of the SAL
545 data revealed increasingly downward trends up to $\sim 4,600$ m a.s.l. in elevation. Above $\sim 4,600$ m a.s.l.
546 this trend is reversed, likely because of permanent or semi-permanent dry snow conditions present in
547 glacier accumulation zone. Snow cover duration (SCD) decreased on average by 43 ± 20 days
548 throughout the study area between 2000 and 2016 with largest changes occurring at elevations below
549 4.500 m a.s.l. on the eastern side and 3.500 m a.s.l. on the western side.

550 TIMESAT was unable to extract SCD for glacier areas that were covered with snow for most of
551 the year due to the lack of seasonal variation. Additionally, in situations of large variations in snow
552 conditions occurring over a very short time period the Savitzky-Golay seasonal fitting process applied
553 may introduce some errors. SCD trends for the study area indicate a shortening of the snow season
554 between 2000 and 2016. SCI trends for the included glacial areas were also shown to be downward
555 during this 16-year observation period (these being more pronounced on the eastern side of the
556 Cordillera).

557 The impact of ENSO events, which influence largescale precipitation and temperature patterns
558 in the study area, on the SCE, SCD, and SAL was shown to be evident. Per-pixel analyses revealed that
559 ENSO positively influences SCE/SAL values most strongly with a one-month time-lag. Data available
560 from the EYE meteorological station, between 2000 and 2016, reveals that the monthly SCE and SAL
561 values are primarily determined by variations in temperature, whilst montly SCI values are determined
562 mostly by precipitation. If the observed decline in SCE persist in the coming years, it will likely result
563 in a a seasonal redistribution of avaiable downstream freshwater which may cause future problems for
564 people and agriculture in the region.

565

566 **Acknowledgements**

567 We extend a special thanks to the editor and the reviewers for their insightful critique of this
568 article. This work was supported by the Chilean Fondecyt Regular Competition under grant agreement

569 #1140172. All data requests should be addressed to the first author. The authors have no conflict of
570 interest.

571

572

573 **References:**

574 Abermann, J., Kinnard, C., & MacDonell, S. (2014). Albedo variations and the impact of clouds on
575 glaciers in the Chilean semi-arid Andes. *Journal of Glaciology*, 60, 183-191

576 Apaloo, J., Brenning, A., & Bodin, X. (2012). Interactions between Seasonal Snow Cover, Ground
577 Surface Temperature and Topography (Andes of Santiago, Chile, 33.5°S). *Permafrost and*
578 *Periglacial Processes*, 23, 277-291

579 Arenson, L.U., Jakob, M., & Wainstein, P. (2015). Effects of Dust Deposition on Glacier Ablation and
580 Runoff at the Pascua-Lama Mining Project, Chile and Argentina. In G. Lollino, A. Manconi, J.
581 Clague, W. Shan, & M. Chiarle (Eds.), *Engineering Geology for Society and Territory - Volume*
582 *1: Climate Change and Engineering Geology* (pp. 27-32). Cham: Springer International
583 Publishing

584 Arsenault, K.R., Houser, P.R., & De Lannoy, G.J.M. (2014). Evaluation of the MODIS snow cover
585 fraction product. *Hydrological Processes*, 28, 980-998

586 Benn, D.I., & Evans, D.J.A. (2010). *Glaciers and glaciation*. London: Hodder Education

587 Bodin, X., Rojas, F., & Brenning, A. (2010). Status and evolution of the cryosphere in the Andes of
588 Santiago (Chile, 33.5 degrees S.). *Geomorphology*, 118, 453-464

589 Box, J.E., Fettweis, X., Stroeve, J.C., Tedesco, M., Hall, D.K., & Steffen, K. (2012). Greenland ice
590 sheet albedo feedback: thermodynamics and atmospheric drivers. *The Cryosphere*, 6, 821-839

591 Box, J.E., Van As, D., Steffen, K., Fausto, R.S., Ahlstrøm, A.P., Citterio, M., & Andersen, S.B. (2017).
592 Greenland, Canadian and Icelandic land-ice albedo grids (2000–2016). *Geol. Surv. Den.*
593 *Greenl. Bull*, 38, 53-56

594 Brock, B.W., Willis, I.C., & Sharp, M.J. (2000). Measurement and parameterization of albedo
595 variations at Haut Glacier d'Arolla, Switzerland. *Journal of Glaciology*, 46, 675-688

596 Burakowski, E.A., Ollinger, S.V., Lepine, L., Schaaf, C.B., Wang, Z., Dibb, J.E., Hollinger, D.Y., Kim,
597 J., Erb, A., & Martin, M. (2015). Spatial scaling of reflectance and surface albedo over a mixed-

598 use, temperate forest landscape during snow-covered periods. *Remote Sensing of Environment*,
599 158, 465-477

600 Cai, W., Borlace, S., Lengaigne, M., van Rensch, P., Collins, M., Vecchi, G., Timmermann, A.,
601 Santoso, A., McPhaden, M.J., Wu, L., England, M.H., Wang, G., Guilyardi, E., & Jin, F.-F.
602 (2014). Increasing frequency of extreme El Nino events due to greenhouse warming. *Nature*
603 *Clim. Change*, 4, 111-116

604 Carey, M., Molden, O.C., Rasmussen, M.B., Jackson, M., Nolin, A.W., & Mark, B.G. (2017). Impacts
605 of Glacier Recession and Declining Meltwater on Mountain Societies. *Annals of the American*
606 *Association of Geographers*, 107, 350-359

607 Casey, K.A., Polashenski, C.M., Chen, J., & Tedesco, M. (2017). Impact of MODIS sensor calibration
608 updates on Greenland Ice Sheet surface reflectance and albedo trends. *The Cryosphere*, 11,
609 1781-1795

610 Cereceda-Balic, F., Palomo-Marín, M.R., Bernalte, E., Vidal, V., Christie, J., Fadic,
611 X., Guevara, J.L., Miro, C., & Pinilla Gil, E. (2012). Impact of Santiago de Chile urban
612 atmospheric pollution on anthropogenic trace elements enrichment in snow precipitation at
613 Cerro Colorado, Central Andes. *Atmospheric Environment*, 47, 51-57

614 Cornwell, E., Molotch, N.P., & McPhee, J. (2016). Spatio-temporal variability of snow water
615 equivalent in the extra-tropical Andes Cordillera from distributed energy balance modeling and
616 remotely sensed snow cover. *Hydrology and Earth System Sciences*, 20, 411-430

617 Corripio, J.G., & Purves, R.S. (2006). Surface Energy Balance of High Altitude Glaciers in the Central
618 Andes: The Effect of Snow Penitentes. *Climate and Hydrology in Mountain Areas* (pp. 15-27):
619 John Wiley & Sons, Ltd

620 Cuffey, K.M., & Paterson, W.S.B. (2010). *The Physics of Glaciers*. Elsevier Science

621 Dariane, A.B., Khoramian, A. & Santi, E. (2017). Investigating spatiotemporal snow cover variability
622 via cloud-free MODIS snow cover product in Central Alborz Region. *Remote Sensing of*
623 *Environment*, 202, 152-165.

624 Delbart, N., Dunesme, S., Lavie, E., Madelin, M., & Goma, R. (2015). Remote sensing of Andean
625 mountain snow cover to forecast water discharge of Cuyo rivers. *Journal of Alpine Research*,
626 15

627 Dozier, J., & Frew, J. (1981). Atmospheric Corrections to Satellite Radiometric Data over Rugged
628 Terrain. *Remote Sensing of Environment*, 11, 191-205

628 Dozier, J., Painter, T.H., Rittger, K., & Frew, J.E. (2008). Time-space continuity of daily maps of
629 fractional snow cover and albedo from MODIS. *Advances in Water Resources*, 31, 1515-1526

630 Dubayah, R. (1992). Estimating Net Solar-Radiation Using Landsat Thematic Mapper and Digital
631 Elevation Data. *Water Resources Research*, 28, 2469-2484

632 Dumont, M., Gardelle, J., Sirguey, P., Guillot, A., Six, D., Rabatel, A., & Arnaud, Y. (2012). Linking
633 glacier annual mass balance and glacier albedo retrieved from MODIS data. *The Cryosphere*, 6,
634 1527-1539

635 Eastman, J.R. (2009). IDRISI Taiga guide to GIS and image processing. *Clark Labs Clark University,*
636 *Worcester, MA*

637 Eklundh, L., & Jönsson, P. (2015). TIMESAT: A Software Package for Time-Series Processing and
638 Assessment of Vegetation Dynamics. In C. Kuenzer, S. Dech, & W. Wagner (Eds.), *Remote*
639 *Sensing Time Series: Revealing Land Surface Dynamics* (pp. 141-158). Cham: Springer
640 International Publishing

641 Escobar, F., Casassa, G., & Pozo, V. (1995). Variaciones de un glaciar de Montaña en los Andes de
642 Chile Central en las últimas dos décadas. *Bulletin de l'Institut français d'études andines*, 24,
643 683-995

644 Falvey, M., & Garreaud, R. (2007). Wintertime Precipitation Episodes in Central Chile: Associated
645 Meteorological Conditions and Orographic Influences. *Journal of Hydrometeorology*, 8, 171-
646 193

647 Falvey, M., & Garreaud, R.D. (2009). Regional cooling in a warming world: Recent temperature trends
648 in the southeast Pacific and along the west coast of subtropical South America (1979-2006).
649 *Journal of Geophysical Research-Atmospheres*, 114

650 Farr, T.G., Rosen, P.A., Caro, E., Crippen, R., Duren, R., Hensley, S., Kobrick, M., Paller, M.,
651 Rodriguez, E., Roth, L., Seal, D., Shaffer, S., Shimada, J., Umland, J., Werner, M., Oskin, M.,
652 Burbank, D., & Alsdorf, D. (2007). The Shuttle Radar Topography Mission. *Reviews of*
653 *Geophysics*, 45, n/a-n/a

654 Fausto, R.S., van As, D., Antoft, J.A., Box, J.E., Colgan, W., & Team, P.P. (2015). Greenland ice sheet
655 melt area from MODIS (2000-2014). *Geological Survey of Denmark and Greenland Bulletin*,
656 57-60

- 657 Gacitua, G., Uribe, J.A., R., W., Loriaux, T., Hernandez, J., & Rivera, A. (2015). 50MHz helicopter-
658 borne radar data for determination of glacier thermal regime in the central Chilean Andes.
659 *Annals of Glaciology*, 56
- 660 Gao, Y., Xie, H.J., Yao, T.D., & Xue, C.S. (2010). Integrated assessment on multi-temporal and multi-
661 sensor combinations for reducing cloud obscuration of MODIS snow cover products of the
662 Pacific Northwest USA. *Remote Sensing of Environment*, 114, 1662-1675
- 663 Gardner, A.S., & Sharp, M.J. (2010). A review of snow and ice albedo and the development of a new
664 physically based broadband albedo parameterization. *Journal of Geophysical Research-Earth*
665 *Surface*, 115
- 666 Garreaud, R.D., Vuille, M., Compagnucci, R., & Marengo, J. (2009). Present-day South American
667 climate. *Palaeogeography Palaeoclimatology Palaeoecology*, 281, 180-195
- 668 Gurung, D. R., Maharjan, S. B., Shrestha, A. B., Shrestha, M. S., Bajracharya, S. R. and Murthy, M. S.
669 R. (2017). Climate and topographic controls on snow cover dynamics in the Hindu Kush
670 Himalaya. *Int. J. Climatol.*, 37: 3873–3882.
- 671 Hall, D.H., & Riggs, G. (2016). MODIS/Terra Snow Cover Daily L3 Global 500m Grid, Version 6. In
672 National Snow and Ice Data Center (NSIDC) (Ed.). Boulder, Colorado USA: NASA
- 673 Hall, D.K., & Riggs, G.A. (2007). Accuracy assessment of the MODIS snow products. *Hydrological*
674 *Processes*, 21, 1534-1547
- 675 Hall, D.K., Riggs, G.A., & Salomonson, V.V. (1995). Development of methods for mapping global
676 snow cover using moderate resolution imaging spectroradiometer data. *Remote Sensing of*
677 *Environment*, 54, 127-140
- 678 Hall, D.K., Riggs, G.A., Salomonson, V.V., DiGirolamo, N.E., & Bayr, K.J. (2002). MODIS snow-
679 cover products. *Remote Sensing of Environment*, 83, 181-194
- 680 Hansen, J., & Nazarenko, L. (2004). Soot climate forcing via snow and ice albedos. *Proceedings of the*
681 *National Academy of Sciences of the United States of America*, 101, 423-428
- 682 Hock, R. (2005). Glacier melt: a review of processes and their modelling. *Progress in Physical*
683 *Geography*, 29, 362-391
- 684 Huang, X., Deng, J., Wang, W., Feng, Q. & Liang, T. (2017). Impact of climate and elevation on snow
685 cover using integrated remote sensing snow products in Tibetan Plateau. *Remote Sensing of*
686 *Environment*, 190, 274-288.

687 Jönsson, P., & Eklundh, L. (2002). Seasonality extraction by function fitting to time-series of satellite
688 sensor data. *Ieee Transactions on Geoscience and Remote Sensing*, *40*, 1824-1832

689 Jönsson, P., & Eklundh, L. (2004). TIMESAT - a program for analyzing time-series of satellite sensor
690 data. *Computers & Geosciences*, *30*, 833-845

691 Justice, C.O., Vermote, E., Townshend, J.R.G., Defries, R., Roy, D.P., Hall, D.K., Salomonson, V.V.,
692 Privette, J.L., Riggs, G., Strahler, A., Lucht, W., Myneni, R.B., Knyazikhin, Y., Running, S.W.,
693 Nemani, R.R., Wan, Z.M., Huete, A.R., van Leeuwen, W., Wolfe, R.E., Giglio, L., Muller, J.P.,
694 Lewis, P., & Barnsley, M.J. (1998). The Moderate Resolution Imaging Spectroradiometer
695 (MODIS): Land remote sensing for global change research. *Ieee Transactions on Geoscience
696 and Remote Sensing*, *36*, 1228-1249

697 Kendall, M.G. (1975). *Rank Correlation Methods*. London: Griffin

698 Klein, A.G., & Stroeve, J. (2002a). Development and validation of a snow albedo algorithm for the
699 MODIS instrument. *Annals of Glaciology, Vol 34, 2002*, *34*, 45-52

700 Klein, A.G., & Stroeve, J. (2002b). Development and validation of a snow albedo algorithm for the
701 MODIS instrument. *Annals of Glaciology*, *34*, 45-52

702 Knap, W.H., Brock, B.W., Oerlemans, J., & Willis, I.C. (1999). Comparison of Landsat TM-derived
703 and ground-based albedos of Haut Glacier d'Arolla, Switzerland. *International Journal of
704 Remote Sensing*, *20*, 3293-3310

705 Konzelmann, T., & Ohmura, A. (1995). Radiative Fluxes and Their Impact on the Energy-Balance of
706 the Greenland Ice-Sheet. *Journal of Glaciology*, *41*, 490-502

707 Leiva, J.C. (1999). Recent fluctuations of the Argentinian glaciers. *Global and Planetary Change*, *22*,
708 169-177

709 Li, C., Su, F., Yang, D., Tong, K., Meng, F. and Kan, B. (2017). Spatiotemporal variation of snow
710 cover over the Tibetan Plateau based on MODIS snow product, 2001–2014. *Int. J. Climatol.*
711 doi:10.1002/joc.5204

712 Li, X., Fu, W., Shen, H., Huang, C. & Zhang, L. (2017). Monitoring snow cover variability (2000–
713 2014) in the Hengduan Mountains based on cloud-removed MODIS products with an adaptive
714 spatio-temporal weighted method. *Journal of Hydrology*, *551*, 314-327.

715 Liang, S.L., Stroeve, J., & Box, J.E. (2005). Mapping daily snow/ice shortwave broadband albedo from
716 Moderate Resolution Imaging Spectroradiometer (MODIS): The improved direct retrieval

717 algorithm and validation with Greenland in situ measurement. *Journal of Geophysical*
718 *Research-Atmospheres*, 110

719 Liston, G.E., & Hiemstra, C.A. (2011). The Changing Cryosphere: Pan-Arctic Snow Trends (1979–
720 2009). *Journal of Climate*, 24, 5691-5712

721 López-Moreno, J.I., Valero-Garcés, B., Mark, B., Condom, T., Revuelto, J., Azorín-Molina, C., Bazo,
722 J., Frugone, M., Vicente-Serrano, S.M., & Alejo-Cochachin, J. (2017). Hydrological and
723 depositional processes associated with recent glacier recession in Yanamarey catchment,
724 Cordillera Blanca (Peru). *Science of the Total Environment*, 579, 272-282

725 Lyapustin, A., Wang, Y., Xiong, X., Meister, G., Platnick, S., Levy, R., Franz, B., Korkin, S., Hilker,
726 T., Tucker, J., Hall, F., Sellers, P., Wu, A., & Angal, A. (2014). Scientific impact of MODIS C5
727 calibration degradation and C6+ improvements. *Atmos. Meas. Tech.*, 7, 4353-4365

728 Male, D.H., & Granger, R.J. (1981). Snow Surface-Energy Exchange. *Water Resources Research*, 17,
729 609-627

730 Malmros, J.K., Mernild, S.H., Wilson, R., Yde, J.C., & Fensholt, R. (2016). Glacier area changes in the
731 central Chilean and Argentinean Andes 1955-2013/14. *Journal of Glaciology*, 62, 391-401

732 Mann, H.B. (1945). Nonparametric Tests Against Trend. *Econometrica*, 13, 245-259

733 Marchane, A., Jarlan, L., Hanich, L., Boudhar, A., Gascoïn, S., Tavernier, A., Filali, N., Le Page, M.,
734 Hagolle, O., & Berjamy, B. (2015). Assessment of daily MODIS snow cover products to
735 monitor snow cover dynamics over the Moroccan Atlas mountain range. *Remote Sensing of*
736 *Environment*, 160, 72-86

737 Masiokas, M.H., Christie, D.A., Le Quesne, C., Pitte, P., Ruiz, L., Villalba, R., Luckman, B.H.,
738 Berthier, E., Nussbaumer, S.U., González-Reyes, Á., McPhee, J., & Barcaza, G. (2016).
739 Reconstructing the annual mass balance of the Echaurren Norte glacier (Central Andes, 33.5° S)
740 using local and regional hydroclimatic data. *The Cryosphere*, 10, 927-940

741 Masiokas, M.H., Villalba, R., Luckman, B.H., Le Quesne, C., & Aravena, J.C. (2006). Snowpack
742 variations in the central Andes of Argentina and Chile, 1951-2005: Large-scale atmospheric
743 influences and implications for water resources in the region. *Journal of Climate*, 19, 6334-
744 6352

745 McClung, D.M. (2013). The effects of El Niño and La Niña on snow and avalanche patterns in British
746 Columbia, Canada, and central Chile. *Journal of Glaciology*, 59, 783-792

747 Mernild, S.H., Beckerman, A.P., Yde, J.C., Hanna, E., Malmros, J.K., Wilson, R., & Zemp, M.
748 (2015a). Mass loss and imbalance of glaciers along the Andes Cordillera to the sub-Antarctic
749 islands. *Global and Planetary Change*, 133, 109-119

750 Mernild, S. H., Liston, G. E., Hiemstra, C. A., Beckerman, A. P., Yde, J. C., and McPhee, J. (2016b).
751 The Andes Cordillera. Part IV: Spatiotemporal freshwater runoff distribution to adjacent seas
752 (1979–2014). *International Journal of Climatology*, 37(7), 3175–3196

753 Mernild, S. H., Liston, G. E., Hiemstra, C. A., Malmros, J. K., Yde, J. C., and McPhee, J. (2016a). The
754 Andes Cordillera. Part I: Snow Distribution, Properties, and Trends (1979–2014). *International*
755 *Journal of Climatology*, 37(4), 1680–1698

756 Mernild, S. H., Liston, G. E., Hiemstra, C. A., Yde, J. C., McPhee, J., and Malmros, J. K. (2016c). The
757 Andes Cordillera. Part II: Rio Olivares Basin Snow Conditions (1979–2014), Central Chile.
758 *International Journal of Climatology*, 37(4), 1699–1715.,

759 Mernild, S.H., Liston, G.G., Kane, D.L., Knudsen, N.F., & Hasholt, B. (2008). Snow, runoff, and mass
760 balance modeling for the entire Mittivakkat Glacier (1998-2006), Ammassalik Island, SE
761 Greenland. *Geografisk Tidsskrift-Danish Journal of Geography*, 108, 121-136

762 Mernild, S.H., Malmros, J.K., Yde, J.C., Wilson, R., Knudsen, N.T., Hanna, E., Fausto, R.S., & van
763 As, D. (2015b). Albedo decline on Greenland's Mittivakkat Gletscher in a warming climate.
764 *International Journal of Climatology*, 35, 2294-2307

765 Meza, F.J., Wilks, D.S., Gurovich, L., & Bambach, N. (2012). Impacts of Climate Change on Irrigated
766 Agriculture in the Maipo Basin, Chile: Reliability of Water Rights and Changes in the Demand
767 for Irrigation. *Journal of Water Resources Planning and Management*, 138, 421-430

768 Montecinos, A., & Aceituno, P. (2003). Seasonality of the ENSO-related rainfall variability in central
769 Chile and associated circulation anomalies. *Journal of Climate*, 16, 281-296

770 Moustafa, S.E., Rennermalm, A.K., Román, M.O., Wang, Z., Schaaf, C.B., Smith, L.C., Koenig, L.S.,
771 & Erb, A. (2017). Evaluation of satellite remote sensing albedo retrievals over the ablation area
772 of the southwestern Greenland ice sheet. *Remote Sensing of Environment*, 198, 115-125

773 Oerlemans, J., Giesen, R.H., & Van den Broeke, M.R. (2009). Retreating alpine glaciers: increased
774 melt rates due to accumulation of dust (Vadret da Morteratsch, Switzerland). *Journal of*
775 *Glaciology*, 55, 729-736

776 Neckel, N., Loibl, D., & Rankl, M. (2017). Recent slowdown and thinning of debris-covered glaciers in
777 south-eastern Tibet. *Earth and Planetary Science Letters*, 464, 95-102

778 Pellicciotti, F., Burlando, P., & Van Vliet, K. (2007). Recent trends in precipitation and streamflow in
779 the Aconcagua River basin, central Chile Glacier mass balance changes and meltwater
780 discharge. In, *Foz do Iguacu*. International Association of Hydrological Sciences: IAHS

781 Peña, H., & Nazarala, B. (1987). Snowmelt-Runoff Simulation Model of a Central Chile Andean Basin
782 with Relevant Orographic Effects. In, *International Association of Hydrological Sciences*
783 (*IAHS*). Vancouver, Canada: IAHS

784 Pfeffer, W.T., Arendt, A.A., Bliss, A., Bolch, T., Cogley, J.G., Gardner, A.S., Hagen, J.-O., Hock, R.,
785 Kaser, G., Kienholz, C., Miles, E.S., Moholdt, G., Mölg, N., Paul, F., Radi, Valentina, Rastner,
786 P., Raup, B.H., Rich, J., & Sharp, M.J. (2014). The Randolph Glacier Inventory: a globally
787 complete inventory of glaciers. *Journal of Glaciology*, 60, 537-552

788 Polk, M.H., Young, K.R., Baraer, M., Mark, B.G., McKenzie, J.M., Bury, J., & Carey, M. (2017).
789 Exploring hydrologic connections between tropical mountain wetlands and glacier recession in
790 Peru's Cordillera Blanca. *Applied Geography*, 78, 94-103

791 Prohaska, F. (1976). The climate of Argentina, Paraguay and Uruguay. In W. Schwerdfeger (Ed.),
792 *World Survey of Climatology* (pp. 13 - 112). New York: Elsevier

793 Ragetti, S., Immerzeel, W.W., & Pellicciotti, F. (2016). Contrasting climate change impact on river
794 flows from high-altitude catchments in the Himalayan and Andes Mountains. *Proceedings of*
795 *the National Academy of Sciences of the United States of America*, 113, 9222-9227

796 Riggs, G.A., Hall, D.K. & Román, M.O. (2017) Overview of NASA's MODIS and Visible Infrared
797 Imaging Radiometer Suite (VIIRS) snow-cover Earth System Data Records. *Earth Syst. Sci.*
798 *Data*, 9, 765-777.

799 Rittger, K., Painter, T.H., & Dozier, J. (2013). Assessment of methods for mapping snow cover from
800 MODIS. *Advances in Water Resources*, 51, 367-380

801 Rutllant, J., & Fuenzalida, H. (1991). Synoptic Aspects of the Central Chile Rainfall Variability
802 Associated with the Southern Oscillation. *International Journal of Climatology*, 11, 63-76

803 Saavedra, F.A., Kampf, S.K., Fassnacht, S.R., & Sibold, J.S. (2016). A snow climatology of the Andes
804 Mountains from MODIS snow cover data. *International Journal of Climatology*

805 Saavedra1, F.A., Kampf, S.k., Fassnacht, S.R., and Sibold, J.S. Changes in Andes Mountains snow
806 cover from MODIS data 2000-2014. *The Cryosphere Discuss.*, [https://doi.org/10.5194/tc-2017-](https://doi.org/10.5194/tc-2017-72)
807 72, in review, 2017.

808 Savitzky, A., & Golay, M.J.E. (1964). Smoothing and Differentiation of Data by Simplified Least
809 Squares Procedures. *Analytical Chemistry*, 36, 1627-1639

810 Sirguey, P., Still, H., Cullen, N.J., Dumont, M., Arnaud, Y., & Conway, J.P. (2016). Reconstructing the
811 mass balance of Brewster Glacier, New Zealand, using MODIS-derived glacier-wide albedo.
812 *The Cryosphere*, 10, 2465-2484

813 Sorman, A.U., Akyurek, Z., Sensoy, A., Sorman, A.A., & Tekeli, A.E. (2007). Commentary on
814 comparison of MODIS snow cover and albedo products with ground observations over the
815 mountainous terrain of Turkey. *Hydrology and Earth System Sciences*, 11, 1353-1360

816 Tedesco, M., Fettweis, X., Mote, T., Wahr, J., Alexander, P., Box, J.E., & Wouters, B. (2013).
817 Evidence and analysis of 2012 Greenland records from spaceborne observations, a regional
818 climate model and reanalysis data. *The Cryosphere*, 7, 615-630

819 Tekeli, A.E., Akyürek, Z., Arda Şorman, A., Şensoy, A., & Ünal Şorman, A. (2005). Using MODIS
820 snow cover maps in modeling snowmelt runoff process in the eastern part of Turkey. *Remote*
821 *Sensing of Environment*, 97, 216-230

822 Vuille, M., Kaser, G., & Juen, I. (2008). Glacier mass balance variability in the Cordillera Blanca, Peru
823 and its relationship with climate and the large-scale circulation. *Global and Planetary Change*,
824 62, 14-28

825 Wang, Z., Schaaf, C.B., Strahler, A.H., Chopping, M.J., Román, M.O., Shuai, Y., Woodcock, C.E.,
826 Hollinger, D.Y., & Fitzjarrald, D.R. (2014). Evaluation of MODIS albedo product (MCD43A)
827 over grassland, agriculture and forest surface types during dormant and snow-covered periods.
828 *Remote Sensing of Environment*, 140, 60-77

829 Warren, S.G., & Wiscombe, W.J. (1980). A Model for the Spectral Albedo of Snow. II: Snow
830 Containing Atmospheric Aerosols. *Journal of the Atmospheric Sciences*, 37, 2734-2745

831 Wilson, R., Mernild, S.H., Malmros, J.K., Bravo, C., & CarriÓN, D. (2016). Surface velocity
832 fluctuations for Glaciar Universidad, central Chile, between 1967 and 2015. *Journal of*
833 *Glaciology*, 62, 847-860

- 834 Wiscombe, W.J., & Warren, S.G. (1980). A Model for the Spectral Albedo of Snow. I: Pure Snow.
835 *Journal of the Atmospheric Sciences*, 37, 2712-2733
- 836 Wolter, K., & Timlin, M.S. (2011). El Niño/Southern Oscillation behaviour since 1871 as diagnosed in
837 an extended multivariate ENSO index (MEI.ext). *International Journal of Climatology*, 31,
838 1074-1087
- 839 Xu, W., Ma, H., Wu, D. & Yuan, W. (2017). Assessment of the Daily Cloud-Free MODIS Snow-Cover
840 Product for Monitoring the Snow-Cover Phenology over the Qinghai-Tibetan Plateau. *Remote*
841 *Sensing*, 9, 585.